Heat Capacity Study of the Abrupt Valence-Detrapping Phase Transition of Mixed-Valence [Mn₃O(O₂CCH₃)₆(py)₃]·py[†]

Motohiro Nakano,[1] Michio Sorai,*,[1] John B. Vincent,[2] George Christou,*,[2] Ho. G. Jang,[3] and David N. Hendrickson*,[4]

The heat capacity of the mixed-valence complex [Mn₃O(O₂CCH₃)₆(py)₃]·py, where py is pyridine, has been measured with an adiabatic calorimeter between 13 and 300 K. A phase transition with a sharp heat capacity peak has been found at 184.65 K. The enthalpy and entropy of the phase transition are $\Delta H = 6460$ J mol⁻¹ and $\Delta S = 35.77$ J K⁻¹ mol⁻¹. From a comparison of the present calorimetric results with the results of single-crystal X-ray diffraction, magnetic susceptibility, and solid-state ²H NMR studies, it is concluded that the phase transition is associated with the onset of rapid intramolecular electron transfer in the mixed-valence Mn₃O complexes and the orientational disordering of the pyridine solvate molecules. The former contribution to ΔS is $R \ln 4$, while the latter is $R \ln 18$, where R is the gas constant. The total entropy gain from these two contributions, $R \ln 72$ (=35.56 J K⁻¹ mol⁻¹), agrees well with the observed ΔS. In the high-temperature valence-detrapped phase each Mn₃O complex is dynamically interconverting between four configurations, where in three cases the "extra" electron resides on one manganese ion and the Mn₃O unit is distorted as an isosceles triangle and in the fourth configuration the Mn₃O unit is a symmetric equilateral triangle that is electronically delocalized. The contribution of $R \ln 18$ results from the disordering of the pyridine solvate molecule about a pseudo-C₆ axis perpendicular to the plane of the pyridine and 3-fold reorientations about the crystallographic C₃ axis where the plane of the pyridine solvate molecule in each of its positions is tipped ~15° off the C₃ axis. Together with the isostructural mixed-valence complex [Fe₃O(O₂CCH₃)₆(py)₃](CHCl₃), the present complex [Mn₃O(O₂CCH₃)₆(py)₃]·py is one of two R32 symmetry trinuclear mixed-valence complexes in which the static electron delocalization state has clearly been found to occur as a constituent in the valence-detrapped phase.

Introduction

Mixed-valence complexes are encountered in various fields of science.[5] Many mixed-valence compounds convert from a valence-trapped to a valence-detrapped state when the temperature is increased. Interestingly, in the solid state the valence-detrapping phenomenon is often associated with a phase transition.[6] Intermolecular interactions affect the ground-state potential energy surface of each complex, trapping it in one vibronic state. When the thermal energy becomes larger than the combined intermolecular interactions, mixed-valence complexes in the solid state cooperatively valence-detrap. Domains of complexes convert from the valence-trapped phase to a phase where the ground-state potential energy surface of each complex is more symmetric (two or more vibronic states at the same energy). Relatively fast tunneling between vibronic states occurs for a complex when it has a symmetric ground-state potential energy surface.

Intramolecular electron transfer between the metal centers in a mixed-valence complex is usually treated by a theory incorporating vibronic interactions such as the PKS theory.[7] The "extra" electron residing on the low-oxidation metal center is coupled with molecular vibrations via the vibronic interaction. In effect, the vibronic interaction induces a pseudo-Jahn-Teller[8] distortion of the molecule, in which the extra electron is localized on one particular metal center. Such a molecule is known to be a representative example of "nonrigid or fluxional molecules", which exhibit large-amplitude intramolecular motion. For example, hindered rotation of a methyl group, the puckering motion of cyclopentane, and pseudorotation of inorganic fluoride molecules are other cases where large-amplitude intramolecular motion occurs. In the case of an isolated mixed-valence molecule, the extra electron itinerates among the metal centers in the complex as a result of large-amplitude molecular vibration with the complex.

However, when the mixed-valence complexes are aggregated in a crystal, the rate of intramolecular electron transfer is seriously affected by environmental effects in the solid-state lattice. If the packing of molecules is very tight in the crystal, intramolecular electron transfer is difficult. On the other hand, when the large-amplitude intramolecular vibration is allowed in the crystal

and intermolecular interactions are appreciable, a cooperative crossover phenomenon between the valence-trapped and the valence-detrapped states is expected to occur. From a viewpoint of lattice dynamics, an assembly consisting of anharmonic oscillators possesses the potential to exhibit a phase transition. In many mixed-valence compounds, this phase transition has the character of an order–disorder transition involving the distortion dipoles that arise from the pseudo-Jahn–Teller distortion in each complex.

The title compound, hexakis(μ-acetato)(μ₃-oxo)tris(pyridine)trimanganese(II,2III)–pyridine [Mn₃O(O₂CCH₃)₆(py)₃]·py, where py is pyridine, belongs to a group of trinuclear basic acetates which are one of the typical mixed-valence compounds that exhibit cooperative phenomena. The iron analogues with various solvate

(1) Osaka University.
(2) Indiana University.
(3) University of Illinois.
(4) University of California at San Diego.
(5) (a) Day, P. *Int. Rev. Phys. Chem.* **1981**, *1*, 149. (b) *Mixed-Valence Compounds, Theory and Applications in Chemistry, Physics, Geology and Biology*, Brown, D. B., Ed.; Reidel: Boston, 1980. (c) Creutz, C. *Prog. Inorg. Chem.* **1983**, *30*, 1–73.
(6) (a) Oh, S. M.; Hendrickson, D. N.; Hassett, K. L.; Davis, R. E. *J. Am. Chem. Soc.* **1984**, *106*, 7984. (b) Oh, S. M.; Hendrickson, D. N.; Hassett, K. L.; Davis, R. E. *J. Am. Chem. Soc.* **1985**, *107*, 8009. (c) Oh, S. M.; Kambara, T.; Hendrickson, D. N.; Sorai, M.; Kaji, K.; Woehler, S. E.; Wittebort, R. J. *J. Am. Chem. Soc.* **1985**, *107*, 5540. (d) Sorai, M.; Kaji, K.; Hendrickson, D. N.; Oh, S. M. *J. Am. Chem. Soc.* **1986**, *108*, 702. (e) Woehler, S. E.; Wittebort, R. J.; Oh, S. M.; Hendrickson, D. N.; Inniss, D.; Strouse, C. E. *J. Am. Chem. Soc.* **1986**, *108*, 2938. (f) Kambara, T.; Hendrickson, D. N.; Sorai, M.; Oh, S. M. *J. Chem. Phys.* **1986**, *85*, 2895. (g) Woehler, S. E.; Wittebort, R. J.; Oh, S. M.; Kambara, T.; Hendrickson, D. N.; Inniss, D.; Strouse, C. E. *J. Am. Chem. Soc.* **1987**, *109*, 1063. (h) Oh, S. M.; Wilson, S. R.; Hendrickson, D. N.; Woehler, S. E.; Wittebort, R. J.; Inniss, D.; Strouse, C. E. *J. Am. Chem. Soc.* **1987**, *109*, 1073. (i) Hendrickson, D. N.; Oh, S. M.; Dong, T.-Y.; Kambara, T.; Cohn, M. J.; Moore, M. F. *Comments Inorg. Chem.* **1985**, *4*, 329. (j) Sorai, M.; Shiomi, Y.; Hendrickson, D. N.; Oh, S. M.; Kambara, T. *Inorg. Chem.* **1987**, *26*, 223. (k) Jang, H. G.; Geib, S. J.; Kaneko, Y.; Nakano, M.; Sorai, M.; Rheingold, A. L.; Montez, B.; Hendrickson, D. N. *J. Am. Chem. Soc.* **1989**, *111*, 173.
(7) (a) Piepho, S. B.; Krausz, E. R.; Schatz, P. N. *J. Am. Chem. Soc.* **1978**, *100*, 2996. (b) Wong, K. Y.; Schatz, P. N. *Prog. Inorg. Chem.* **1981**, *28*, 369.
(8) Bersuker, I. B. *The Jahn-Teller Effect and Vibronic Interactions in Modern Chemistry*; Plenum: New York, 1984.
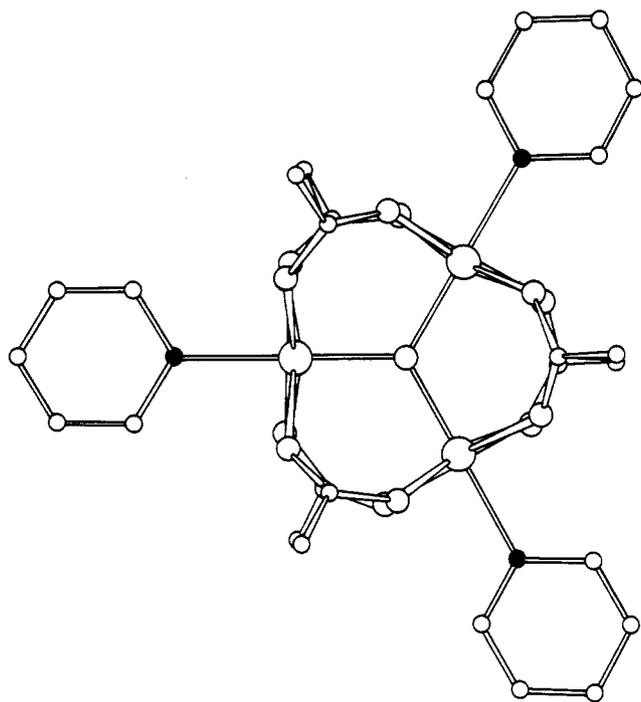
Figure 1. Molecular structure of $[Mn_3O(O_2CCH_3)_6(py)_3]$ in the high-temperature phase. The molecule has 32 symmetry.

molecules have been extensively investigated and many of them are known to exhibit phase transitions associated with the mixed-valence phenomenon.[6] These studies have revealed an important role for the solvate molecules in the lattice. They may assist the intramolecular electron transfer not only as a spacer in the lattice making room for the large-amplitude motion but also as an interaction path between mixed-valence complexes, a pathway that is modulated by reorientational motion of the solvate molecules.

The mixed-valence phenomena in the present manganese compound has already been investigated by means of single-crystal X-ray diffraction, differential scanning calorimetry (DSC), and magnetic susceptibility measurements.[9] No discontinuity was detected in the magnetic susceptibility measurements to indicate the presence of a phase transition; however, the DSC thermogram clearly showed an endothermic peak due to a phase transition at 184.7 K. Moreover, the structural analysis at 223 K revealed[9] that $[Mn_3O(O_2CCH_3)_6(py)_3]$·py crystallizes in rhombohedral space group $R32$ and a 3-fold axis passing through the complex molecules exists (see Figure 1). This fact indicates that on the long time scale of the X-ray diffraction technique the three manganese ions are equivalent; that is, the valence-detrapped phase has been established in the complex molecule at 223 K. The X-ray structural results also indicated that below ~190–200 K the crystallographic C_3 axis disappears.

The main purpose of this paper is to determine accurate heat capacity data for $[Mn_3O(O_2CCH_3)_6(py)_3]$·py and to elucidate, on the basis of transition entropy, what kinds of molecular degrees of freedom are responsible for the phase transition.

Experimental Section

Compound Preparation. The original sample of [Mn₃O(O₂CCH₃)₆-(py)₃]·py was prepared according to the method previously described.[9] This original sample will be designated hereafter as sample 1. Sample 1 exhibited three peaks at 173.5, 184.7, and 258.5 K in the heat capacity measurements. Although the main peak at 184.7 K agrees well with the anomaly detected by DSC,[9] the other two peaks were not observed in the DSC run. We thought that sample 1 might contain some chemical impurities, in particular, a complex with less than a stoichiometric amount of pyridine solvate molecules. In fact, as shown in Table I, the results of elemental analysis for sample 1 compare favorably with the

Table I. Elemental Analyses for $[Mn_3O(O_2CCH_3)_6(py)_3]$·$x$py

	C	H	N
		%	
	Calcd		
x = 1.00	45.14	4.50	6.58
x = 0.89	44.82	4.48	6.46
x = 0.70	44.26	4.44	6.26
	Found		
sample 1	44.30	4.38	6.36
sample 2 (batch 1)	44.83	4.47	6.46
sample 2 (batch 2)	45.06	4.53	6.57
sample 3	45.16	4.47	6.54
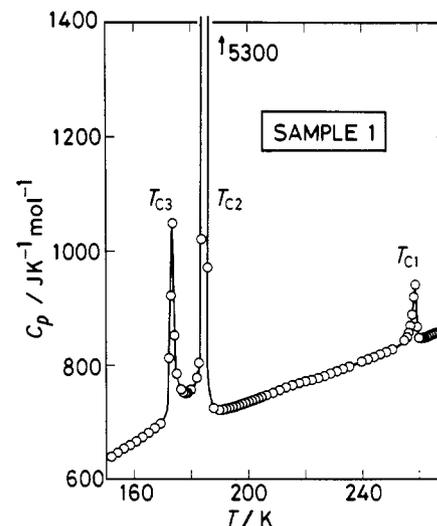
Figure 2. Molar heat capacity of sample 1 of $[Mn_3O(O_2CCH_3)_6(py)_3]$·py in the vicinity of the phase transitions.

calculated values for x = 0.70 rather than x = 1.00, where x is the average content of the pyridine solvate molecule per complex.

Therefore, sample 1 was recrystallized from pure pyridine in two batches. The amount of crystallites obtained in batches 1 and 2 were 8.0 and 7.5 g, respectively, and the combination of these two batches will be designated as sample 2. As expected, the two subsidiary peaks detected in sample 1 disappeared from sample 2. However, the peak due to the phase transition split into a doublet centered at 184.2 and 184.62 K. We thought that the splitting of the transition peak might be caused by the different qualities of the crystals prepared in batches 1 and 2. Close examination of the elemental analyses (see Table I) indicates that batch 1 consists of a complex with less pyridine solvate (x = 0.89), while batch 2 contains the complex with x = 1.00.

Sample 2 was then carefully recrystallized from pure pyridine in a single batch. The elemental analyses (Table I) showed that sample 3 consists of the complexes with x = 1.00. Heat capacity measurements for sample 3 showed a single phase transition at 184.68 K.

Heat Capacity Measurements. Heat capacities were measured with an adiabatic calorimeter[10] between 13 and 300 K. A calorimeter cell was loaded with 22.4045, 15.3909, and 16.4451 g of samples 1, 2, and 3, respectively, after buoyancy correction in which the density of the sample was 1.456 cm⁻³. A small amount of helium gas was sealed in the cell to aid in heat transfer.

Results and Discussion

Calorimetric measurements were evaluated in terms of C_p, the molar heat capacity under constant pressure. The heat capacities for sample 1 are plotted in Figure 2 over the range from 150 to 270 K. Three phase transitions were observed at T_{C_3} = 173.5 K, T_{C_2} = 184.7 K, and T_{C_1} = 258.5 K. The transition enthalpy and entropy for the respective phase transitions were evaluated to be ΔH = 1880 J mol⁻¹ and ΔS = 11.43 J K⁻¹ mol⁻¹ for the transition at T_{C_3}, 4290 J mol⁻¹ and 23.00 J K⁻¹ mol⁻¹ for the transition T_{C_2}, and 260 J mol⁻¹ and 1.00 J K⁻¹ mol⁻¹ for the transition at T_{C_1}. Although the main phase transition at T_{C_2} agrees well with the

(9) Vincent, J. B.; Chang, H.-R.; Folting, K.; Huffman, J. C.; Christou, G.; Hendrickson, D. N. *J. Am. Chem. Soc.* **1987**, *109*, 5703.

(10) Construction of an adiabatic calorimeter workable between 13 and 523 K: Sorai, M.; Kaji, K. Unpublished results.
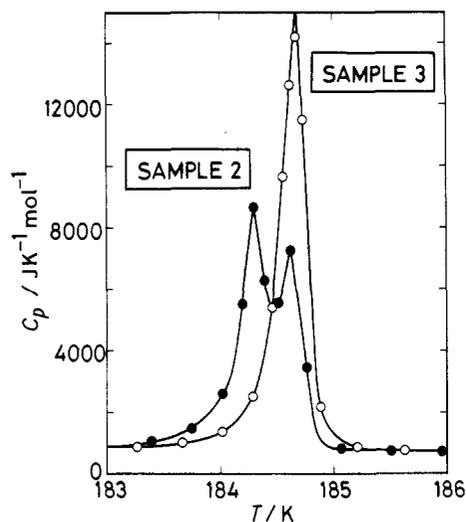
Figure 3. Molar heat capacities of samples 2 and 3 of [Mn₃O-(O₂CCH₃)₆(py)₃]·py in the vicinity of the phase transition.

anomaly previously detected by DSC,[9] the existence of the two extra phase transitions at T_{C_1} and T_{C_3} is inconsistent with the results of DSC. As described in the previous section, sample 1 probably consists of complexes with different amounts of the pyridine solvate molecule.

Sample 2, which is the recrystallized form of sample 1, exhibited a sharp heat capacity peak around 184 K; the two extra peaks observed for sample 1 at T_{C_1} and T_{C_3} completely disappeared from the C_p versus temperature curve of sample 2. The maximum C_p value at the phase transition point, $C_p(\text{max})$, was found to be ~8650 J K⁻¹ mol⁻¹, which is much larger than ~5300 J K⁻¹ mol⁻¹ for sample 1 at T_{C_2}. However, as shown in Figure 3, the C_p peak is split into two peaks centered at T_{C_2} = 184.29 K and T_{C_1} = 184.62 K. The $C_p(\text{max})$ values at T_{C_2} and T_{C_1} are ~8650 and ~7240 J K⁻¹ mol⁻¹, respectively. The total enthalpy and entropy of this double-peaked phase transition are ΔH = 6470 J mol⁻¹ and ΔS = 37.02 J K⁻¹ mol⁻¹, respectively. Since the temperature difference between the two peaks is as small as 0.33 K, it is very likely that the double peak is attributable to a slight difference in content of the pyridine solvate molecule between the two batches which comprise sample 2. Elemental analyses indicate that the average content of the pyridine solvate molecule per complex is 0.89 and 1.00 for batches 1 and 2, respectively. This fact suggests an important role played by the solvate molecules for the mechanism of the phase transition. In relation to this, it should be remarked that the unsolvated analogue did not show any thermal anomaly in the DSC thermogram.[9]

It was decided, therefore, to obtain a homogeneous sample with a stoichiometric amount of pyridine solvate molecules. Sample 2 and 3.5 g of newly prepared sample were then dissolved in pure pyridine, and the solvent was carefully evaporated. The crystallites were filtered out and washed with pyridine. The compound thus prepared was dried under a stream of dry nitrogen gas. This sample is designated as sample 3. As shown in Table I, the results of elemental analyses agree well with the calculated values for the complex with one pyridine solvate molecule per complex.

The molar heat capacities of sample 3 are listed in Table II and plotted in Figure 4 over the whole temperature range studied. A very sharp single peak arising from the phase transition was observed at 184.68 K. The peak height was found to be $C_p(\text{max})$ = 14 190 J K⁻¹ mol⁻¹, which is much higher than ~5300 for sample 1 and ~8650 J K⁻¹ mol⁻¹ for sample 2 (see Figure 3). The transition temperature (184.68 K) for sample 3 just coincides with 184.62 K corresponding to one of the double peaks for sample 2. This fact again supports the suggestion that the phase transition at T_{C_1} is attributable to the complex with x = 1.00, while the transition at T_{C_2} is due to the complex with x = 0.89. Heat capacity measurements carried out across the phase transition were repeated (series 2). As shown in Figure 5, the series 2 measurements gave the phase transition at 184.61 K, which is 0.07
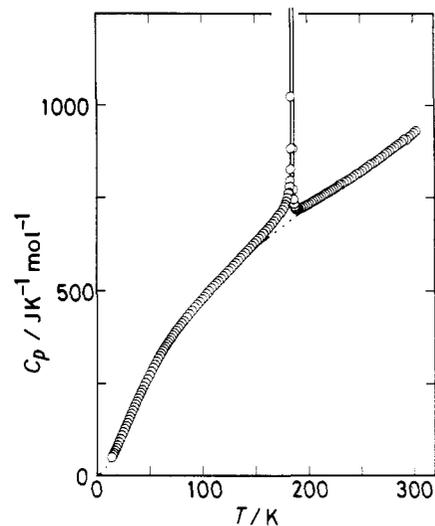
Figure 4. Molar heat capacity of sample 3 of [Mn₃O(O₂CCH₃)₆(py)₃]·py over the whole temperature range studied. The broken curve represents the sum of the magnetic contribution and the lattice heat capacity.
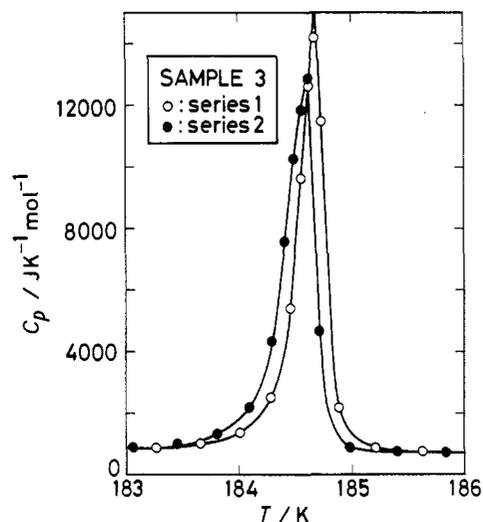
Figure 5. Molar heat capacity of sample 3 of [Mn₃O(O₂CCH₃)₆(py)₃]·py in the vicinity of the phase transition. The series 2 data were collected after the series 1 data.

deg lower than the transition point detected in the series 1 measurements. Moreover, $C_p(\text{max})$ = 12,870 J K⁻¹ mol⁻¹ for series 2 is slightly lower than that found for series 1. Since this kind of shift in the transition temperature has not been observed for other mixed-valence complexes with $R32$ symmetry,[6] it is likely that local strain in the freshly prepared crystallites was released by repeating the phase transition. At any rate, both series of the measurements showed the very sharp phase transition occurring in the temperature interval of less than 1 K. It must be emphasized that the small change in C_p peak from the series 1 to series 2 measurements is in no way attributable to the adiabatic calorimeter, which is quite stable. Furthermore, the sample history dependencies described above are quite reasonable in view of the fact that there is considerable first-order character in the phase transition of [Mn₃O(O₂CCH₃)₆(py)₃]·py. It is well-known that the properties of first-order phase transitions are sample history dependent. As will be described in detail below, the first-order phase transition in this Mn₃O complex involves, in part, a cooperative onset of dynamics associated with the pyridine solvate molecules; thus, the amount of solvate molecule in a given sample is quite critical.

In order to determine the thermodynamic quantities associated with the phase transition, a "normal" heat capacity curve was estimated by the following procedure. At first, the magnetic contribution was subtracted from the observed heat capacities by employing the intracluster magnetic exchange parameters eval-

Table II. Molar Heat Capacities of [Mn₃O(O₂CCH₃)₆(py)₃]·py (Sample 3)

T/K	C_p/J K⁻¹ mol⁻¹	T/K	C_p/J K⁻¹ mol⁻¹	T/K	C_p/J K⁻¹ mol⁻¹	T/K	C_p/J K⁻¹ mol⁻¹	T/K	C_p/J K⁻¹ mol⁻¹
				Series 1					
14.007	50.549	61.946	338.480	133.993	582.72	184.553	9632.9	225.939	776.60
14.967	56.564	63.288	344.654	136.229	589.74	184.619	12612	227.813	780.97
15.930	61.540	64.598	350.323	138.445	596.32	184.674	14188	229.682	785.14
17.008	68.491	65.878	356.104	140.641	602.84	184.731	11480	231.546	786.60
18.210	75.554	67.132	361.361	142.819	609.43	184.884	2178.9	233.717	791.77
19.400	82.979	68.480	367.046	144.979	616.09	185.208	883.35	236.191	795.15
20.689	91.285	69.976	373.336	147.122	622.92	185.624	772.43	238.657	799.51
22.071	100.172	71.538	380.029	149.248	629.28	186.055	746.02	241.113	804.75
23.420	109.692	73.162	386.757	151.358	635.74	186.491	734.01	243.560	809.59
24.760	118.207	74.849	393.144	153.453	642.13	186.928	726.93	245.997	814.47
26.074	126.917	76.592	400.050	155.533	648.55	187.367	722.50	248.433	818.06
27.374	135.406	78.391	406.82	157.598	655.07	187.807	720.13	250.854	823.07
28.623	143.574	80.201	413.53	159.711	661.61	188.246	719.98	253.265	828.17
29.873	151.996	82.026	419.97	161.748	667.94	188.686	718.91	255.668	833.04
31.129	160.301	84.787	429.85	163.771	674.59	189.125	720.87	258.061	839.91
32.379	169.179	87.235	438.61	165.781	681.52	189.565	718.14	260.445	842.96
33.701	177.544	89.770	447.32	167.777	688.16	190.003	719.55	262.823	846.81
35.015	186.377	92.249	455.86	169.761	695.85	191.214	720.24	265.195	851.78
36.248	194.665	94.677	463.37	171.731	704.34	193.194	722.55	267.557	856.93
27.477	202.447	97.059	470.89	173.689	710.60	195.168	725.41	269.912	861.46
38.753	210.643	99.398	478.14	175.634	718.72	197.136	728.18	272.258	867.30
40.012	218.512	101.698	485.37	177.085	726.59	199.097	730.98	274.596	872.44
41.290	226.255	104.020	492.94	178.047	732.97	201.053	734.34	276.928	876.91
42.586	234.034	106.396	500.44	179.004	741.05	203.002	737.67	279.252	881.77
44.118	243.253	108.737	507.58	179.954	751.13	204.945	741.23	281.569	886.38
45.864	253.223	111.045	514.56	180.898	762.28	206.883	744.22	283.878	891.45
47.672	263.618	113.322	520.99	181.584	763.91	208.814	747.21	286.178	895.85
49.541	274.181	115.571	527.33	182.013	780.45	210.740	750.18	288.469	901.12
51.314	284.335	117.793	533.71	182.439	796.36	212.659	753.41	290.750	907.54
53.006	293.930	120.095	540.43	182.859	827.58	214.573	756.90	293.021	908.10
54.628	302.476	122.475	547.82	183.269	884.33	216.481	760.28	295.286	914.48
56.188	310.616	124.827	555.01	183.660	1023.8	218.384	763.48	297.549	919.73
57.695	318.138	127.154	561.75	184.011	1368.0	220.281	766.81	299.804	926.56
59.153	325.333	129.457	569.03	184.283	2510.8	222.172	770.13	302.053	931.56
60.569	332.218	131.736	575.92	184.455	5407.2	224.058	773.32		
				Series 2					
168.017	689.37	179.251	743.02	184.094	2194.3	185.396	762.32	188.907	718.45
170.015	697.08	180.196	756.86	184.288	4336.1	185.830	735.40	189.346	719.21
172.000	705.32	181.132	774.45	184.407	7568.8	186.268	727.60	189.785	719.46
173.476	709.72	181.811	785.93	184.488	10260	186.707	723.17	190.225	719.92
174.448	713.52	182.236	803.12	184.553	11842	187.147	721.15	191.483	720.93
175.416	717.90	182.655	830.22	184.612	12866	187.587	719.43	193.557	722.33
176.381	722.58	183.064	896.17	184.710	4663.0	188.027	718.84	195.625	725.63
177.342	727.64	183.454	1019.6	184.980	890.94	188.467	718.73	197.686	728.66
178.299	733.76	183.808	1328.3						

Table III. Thermodynamic Quantities Associated with the Phase Transition of [Mn₃O(O₂CCH₃)₆(py)₃]·py (Sample 3)

series	T_C/K	$\Delta_{trs}H$/kJ mol⁻¹	$\Delta_{trs}S$/J K⁻¹ mol⁻¹
1	184.68	6.438	35.66
2	184.61	6.475	35.88

uated in the magnetic susceptibility measurements.[9] The residual heat capacities in the temperature ranges 30–120 and 240–270 K, where the phase transition does not seem to exert its effect, were used for an estimate of the lattice heat capacity containing the contributions from intramolecular and lattice vibrations by means of regression calculation for the effective frequency spectrum method.[11] The sum of the magnetic and vibrational contributions forms the normal heat capacities, which are shown in Figure 4 by the broken curve. The transition enthalpy corresponds to the area bounded by the observed and normal heat capacity curves, while the transition entropy was calculated by integrating the excess heat capacity (i.e., that exceeding the normal heat capacity curve) with respect to ln T. The thermodynamic quantities thus determined are $\Delta H = 6440$ J mol⁻¹ and $\Delta S = 35.66$ J K⁻¹ mol⁻¹ for series 1 while $\Delta H = 6480$ J mol⁻¹ and $\Delta S = 35.88$ J K⁻¹ mol⁻¹ for series 2. For a discussion given below, we shall adopt the average quantities, that is, $T_C = 184.65$ K, $\Delta H = 6460$ J mol⁻¹, and $\Delta S = 35.77$ J K⁻¹ mol⁻¹.

(11) Sorai, M.; Seki, S. *J. Phys. Soc. Jpn.* **1972**, *32*, 382.
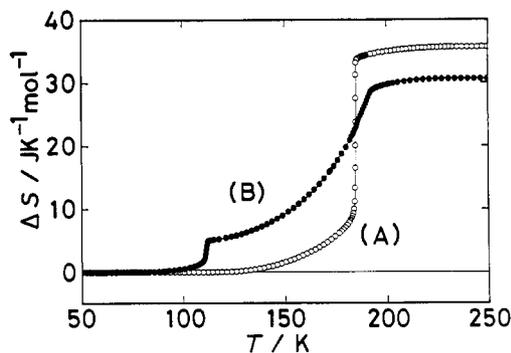
Figure 6. Acquisition of the excess entropy (ΔS) arising from the phase transitions of (A) [Mn₃O(O₂CCH₃)₆(py)₃]·py and (B) [Fe₃O-(O₂CCH₃)₆(py)₃]·py. The heat capacity data for sample 3 of the Mn₃O complex were used to calculate the ΔS versus temperature plot for this complex.

The temperature-dependence of the excess entropy arising from the phase transition is shown in Figure 6. The saturation value at the high-temperature side corresponds to the transition entropy. The abrupt entropy gain at the transition temperature, which is characteristic of a first-order phase transition, turns out to be about 24 J K⁻¹ mol⁻¹. This quantity agrees well with the 24.7 J K⁻¹ mol⁻¹ value obtained from the DSC measurement.[9] However, the present adiabatic calorimetry (see Figures 4 and 6) has revealed that the

entropy gain below the transition temperature is also significant in addition to the first-order transition component. The total observed calorimetric entropy (35.77 J K^{-1} mol^{-1}) is about 145% of the 24.7 J K^{-1} mol^{-1} value obtained from the thermal analysis (DSC). This is due to the fact that it is generally difficult for thermal analysis to detect a sluggish heat capacity anomaly, and hence the DSC thermogram[9] recorded mainly only the first-order contribution.

Degrees of Freedom Accessed in the Phase Transition of [Mn₃O(O₂CCH₃)₆(py)₃]·py. The entropy gain observed for the phase transition of [Mn$_3$O(O$_2$CCH$_3$)$_6$(py)$_3$](py) may be interpreted in terms of two contributions: one is the valence detrapping in the mixed-valence complex and the other is reorientational motion of the pyridine solvate molecule. First, the contribution from the former is discussed. Although direct observation of intramolecular electron transfer by means of Mössbauer spectroscopy is not possible for the present manganese compound as it was for [Fe$_3$O(O$_2$CCH$_3$)$_6$(py)$_3$]·py,[6g] three experimental facts confirm that the phase transition at 184.65 K is associated with the valence-detrapping phenomenon in the Mn$_3$O complex. As described above, the first evidence is that the X-ray structural analysis[10] revealed the equivalence of the three manganese atoms in a complex molecule in the high-temperature phase. This indicates that the valence-detrapped state has been established in the complex at temperatures above 223 K. The second evidence is that the low-temperature behavior of the magnetic susceptibility has been well accounted for in terms of the Heisenberg–Dirac–Van Vleck (HDVV) model, which assumes a valence-trapped state.[9] The most direct evidence that the 184.65 K phase transition involves valence detrapping comes from solid-state ^{2}H NMR experiments[12] carried out on a single crystal of [Mn$_3$O-(O$_2$CCD$_3$)$_6$(py)$_3$]·py, where the acetate ligands are deuterated. When the single crystal was oriented at room temperature with the magnetic field parallel to the crystallographic C_3 axis, only one quadrupole-split ^{2}H NMR doublet was seen. All six acetate CD$_3$ groups are equivalent because the Mn$_3$O complexes are rapidly interconverting between their four configurations (vide infra). Upon cooling of the single crystal below $\sim$190 K, the spectrum changed abruptly from one doublet to $\sim$6 doublets. There is clearly a very abrupt valence trapping occurring at the phase transition.

The entropy gain due to the valence-detrapping phenomenon is straightforwardly related to the change in the number of microscopic states that are thermally accessible for the Mn$_3$O complex. Here the microscopic states for one molecule stand for the configurations that a molecule can take. Molecular configurations in the crystal are determined by the force field acting on each atom in a molecule. The force field mainly consists of two contributions: one arises from the valence electrons, i.e., the adiabatic potential, and the other comes from neighboring molecules, i.e., the environmental effects. In what follows, this effective force field will be designated as the mean-field potential. The number of microscopic states corresponds to the number of accessible (by tunneling or thermal activation) minima on the mean-field potential surface of the complex. The adiabatic potential for the trinuclear mixed-valence complex, which is the dominant factor of the mean-field potential, has been studied in detail by use of the tight-binding Hamiltonian.[6f,13–16] According to those calculations, the number of minima on the adiabatic potential surface can be 1, 3, or 4 depending on the interaction parameter $\Delta \equiv kw/\lambda^2$, where w is the electron-transfer integral between two metal ions, λ gauges the strength of the vibronic interaction, and the force constant for the molecular distortion

is k. When $0 < \Delta < \frac{2}{3}$, there are three equal-energy minima on the potential energy surface as pictured in Figure 7a for the case of $\Delta = 0.05$. These three configurations correspond to the "extra" electron being trapped on one of the three Mn ions and the Mn^{II}Mn^{III}$_2$ unit adopts an isosceles triangular form. When Δ is in the range $\frac{2}{3} < \Delta < 0.761$, a fourth minimum appears on the potential energy surface as pictured in Figure 7b for the case of $\Delta = 0.74$. This fourth configuration corresponds to a Mn$_3$O complex that has an equilateral triangular form, and the "extra" electron is delocalized over all three manganese ions.

In the low-temperature phase of [Mn$_3$O(O$_2$CCH$_3$)$_6$(py)$_3$]·py all of the complexes are valence-trapped and have statically one of the isosceles triangular configurations. The sense of distortion of each Mn$_3$O complex is determined by intermolecular interactions. In effect, intermolecular interactions introduce a zero-point energy difference such that one of the distorted-triangle configurations is at a lower energy than any of the other configurations. The "Mexican hat" mean-field potential becomes asymmetric with one minimum at a lower energy than the others. The Mn$_3$O complex becomes valence-trapped in this one lowest energy minimum. Furthermore, the sense of distortion is aligned from one Mn$_3$O complex to another in the low-temperature phase. Hence, the number of the microscopic states is 1 in the low-temperature phase.

Abruptly at the phase transition all of the Mn$_3$O complexes convert from being statically valence-trapped in one lowest energy configuration on an asymmetric "Mexican hat" potential to dynamically moving between all the configurations on a *symmetric* "Mexican hat" potential. The mean-field potential energy surface becomes symmetric because the thermal energy exceeds the collective ligand pyridine–pyridine intermolecular interactions and the pyridine solvate molecules very abruptly convert from being statically fixed in one position to dynamically moving such that they present on the average a C_3 environment about each Mn$_3$O complex. Depending on the magnitude of Δ, the dynamically interconverting Mn$_3$O complexes in the high-temperature phase will either gain access to *three* microscopic states as shown in Figure 7a or to *four* microscopic states as shown in Figure 7b. In the former case the valence detrapping gives an entropy gain of R ln 3 ($=9.13$ J K^{-1} mol^{-1}), whereas in the latter case the entropy gain is R ln 4 ($=11.53$ J K^{-1} mol^{-1}).

Solid-state ^{2}H NMR experiments[12] carried out on the Mn$_3$O complex definitively demonstrated not only that this complex abruptly valence-detraps at the phase transition but also that the pyridine solvate molecules abruptly convert from being static to being dynamic. Variable-temperature ^{2}H NMR experiments were carried out on single-crystal and polycrystalline samples of [Mn$_3$O(O$_2$CCH$_3$)$_6$(C$_5$D$_5$N)$_3$]·C$_5$D$_5$N. Since only one quadrupole-split doublet was seen for the pyridine solvate molecules at temperatures above the phase transition, it was concluded that each pyridine solvate molecule is rapidly rotating about its local pseudo-C_6 axis. In addition, to explain the observed magnitude of residual quadrupole coupling, the plane of each pyridine solvate jumps between three positions distributed about the crystallographic C_3 axis (i.e., the stacking axis for Mn$_3$O complexes). In each of the three positions about the C_3 axis the pyridine plane is tipped off the C_3 axis by $\sim$15°. Each pyridine solvate molecule converts at the phase transition temperature from statically sitting in one position to dynamically moving between 18 distinguishable configurations. The entropy gain contributed by the onset of dynamics of pyridine solvate molecules is R ln 18 ($=24.03$ J K^{-1} mol^{-1}).

The observed entropy associated with the phase transition of [Mn$_3$O(O$_2$CCH$_3$)$_6$(py)$_3$]·py obviously comprises the two contributions described above. Since the observed entropy gain is ΔS = 35.77 J K^{-1} mol^{-1} ($=R$ ln 73.9), the reorientational motion of the pyridine solvate molecule is fully excited; that is, both the in-plane reorientation about the pseudo-C_6 axis and the reorientation about the crystallographic C_3 axis must contribute to the observed ΔS. The contribution from valence detrapping is either R ln 3 or R ln 4. Thus, the total theoretical value for the phase transition is either $\Delta S = R$ ln 3 + R ln 18 = R ln 54 ($=33.17$

(12) Jang, H. G.; Vincent, J. B.; Nakano, M.; Huffman, J. C.; Christou, G.; Sorai, M.; Wittebort, R. J.; Hendrickson, D. N. *J. Am. Chem. Soc.* **1989**, *111*, 7778–7784.
(13) Borshch, S. A.; Kotov, I. N.; Bersuker, I. B. *Chem. Phys. Lett.* **1982**, *89*, 381.
(14) Launay, J. P.; Babonneau, F. *Chem. Phys.* **1982**, *67*, 295.
(15) Cannon, R. D.; Montri, N.; Brown, D. B.; Marshall, K. M.; Elliott, C. M. *J. Am. Chem. Soc.* **1984**, *106*, 2591.
(16) Liehr, A. D. *J. Phys. Chem.* **1963**, *67*, 471.
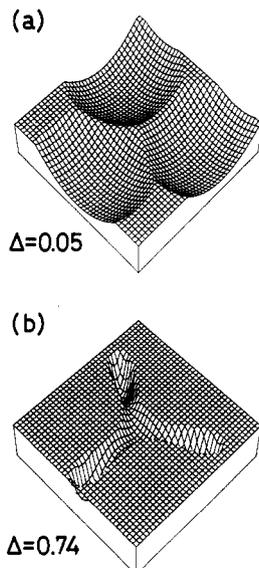
Figure 7. Adiabatic potential energy surface for the ground state of a mixed-valence M$_3$O complex calculated for two different values of $\Delta = kw/\lambda^2$, where w is the electron-transfer integral between two metal ions, λ gauges the strength of the vibronic interaction, and the force constant for the molecular distortion is k. Surface a is for $\Delta = 0.5$ and surface b is for $\Delta = 0.74$.

J K^{-1} mol^{-1}) or $\Delta S = R \ln 4 + R \ln 18 = R \ln 72$ (=35.56 J K^{-1} mol^{-1}). The observed value, $\Delta S = 35.77$ J K^{-1} mol^{-1}, agrees very well with the latter rather than the former possibility. It can be concluded that [Mn$_3$O(O$_2$CCH$_3$)$_6$(py)$_3$]·py valence-detraps at 184.65 K and above this temperature the complex is dynamically interconverting between four configurations, one of which is electronically delocalized.

Nature of the Phase Transition. The most interesting finding in this study is that the valence-detrapping phase transition for [Mn$_3$O(O$_2$CCH$_3$)$_6$(py)$_3$]·py occurs very abruptly as a first-order phase transition at 184.65 K, whereas isostructural [Fe$_3$O-(O$_2$CCH$_3$)$_6$(py)$_3$]·py exhibits two phase transitions, a first-order one at $\sim$112 K with $\Delta S = 4.61$ J K^{-1} mol^{-1} ($\simeq R \ln 2$) and a higher order phase transition that starts at $\sim$115 K and culminates at $\sim$190 K with $\Delta S = 26.04$ J K^{-1} mol^{-1} ($\simeq R \ln 18$). The higher order phase transition has been shown to involve both the conversion of the Fe$_3$O complex from valence-trapped to valence-detrapped as well as the onset of motion of the pyridine solvate molecule. Why does the valence detrapping occur in a first-order phase transition for the Mn$_3$O complex while a higher order phase transition is involved in the case of the Fe$_3$O complex? The dramatic difference between these two isostructural complexes is underscored in Figure 6, where ΔS versus temperature is plotted for both of the complexes. It can be seen that, in comparison to the Fe$_3$O case, transition entropy is gained very abruptly for the Mn$_3$O complex. There is considerably more long-range order (cooperativity) in the valence detrapping for the Mn$_3$O complex.

There have been reported two statistical mechanical theoretical papers[6f,17] dealing with the phase transitions seen for these mixed-valence trinuclear complexes. The pyridine–pyridine intermolecular interactions have been treated by the molecular field approximation. Unfortunately, neither of the two theories have taken into account the role of the solvate molecules. Stratt and Adachi[17] took the insightful approach of employing a "spin" type Hamiltonian, which leads logically to the idea of two interpenetrating sublattices of M$_3$O complexes. Figure 8 shows the phase diagram calculated with this theory, where J_1 and J_2 are parameters that gauge the pairwise intermolecular interactions (via pyridine–pyridine contacts) in which two neighboring M$_3$O complexes are distorted parallel to each other or only one is distorted, respectively. At low temperatures phase I (ferrodistortive phase)

(17) Stratt, R. M.; Adachi, S. H. *J. Chem. Phys.* **1987**, *86*, 7156.
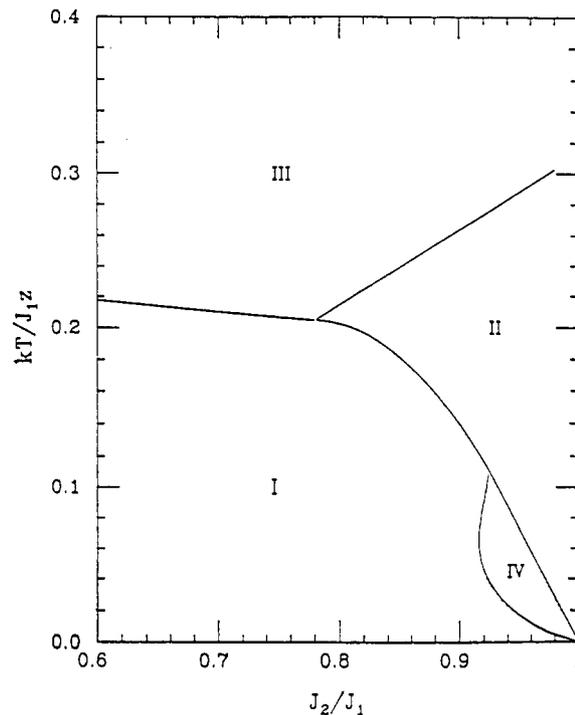
Figure 8. Phase diagram calculated by Stratt and Adachi[17] employing a mean-field theory to account for the phase transitions in mixed-valence Fe$_3$O complexes that crystallize in the $R32$ space group. The vertical axis is temperature plotted in units of $J_1 z/k$, where k is the Boltzmann constant, z is the number of Fe$_3$O complexes surrounding each Fe$_3$O complex, and J_1 is the interaction energy of two neighboring complexes, both of which are distorted parallel to each other. The horizontal axis is the ratio of the "antiferromagnetic" (J_2) to the "ferromagnetic" (J_1) coupling, where J_2 is the interaction energy for two neighboring complexes, one of which is distorted and the other is undistorted.

exists, where all M$_3$O complexes are valence-trapped and, because of strain dipoles, the sense of distortion of each M$_3$O complex is the same. In phase II (antidistortive phase) two interpenetrating sublattices exist where one sublattice has valence-trapped complexes and the sense of distortion (i.e., which ion is the M^{II} ion) is random. The other sublattice has an appreciable number of undistorted (delocalized) complexes mixed with randomly oriented valence-trapped complexes. In phase III (paradistortive phase) there is a random distribution of distorted and undistorted complexes, where each M$_3$O complex is probably tunneling rapidly between its four configurations. In Figure 8 it is important to note that only the phase boundaries involving I–III, I–II, and IV–II phases correspond to first-order transitions. The other lines correspond to second-order transitions.

An explanation for the differences in phase transition behavior between [Mn$_3$O(O$_2$CCH$_3$)$_6$(py)$_3$]·py and [Fe$_3$O(O$_2$CCH$_3$)$_6$-(py)$_3$]·py can be gleaned from Figure 8. It should be remarked here that although in the calorimetric study on [Fe$_3$O-(O$_2$CCH$_3$)$_6$(py)$_3$]·py[6d] the existence of the undistorted configuration was not claimed, we shall assume, in order to apply Stratt and Adachi's theoretical model[17] to both complexes, that all four configurations would also be realized in the Fe$_3$O complex. If J_2/J_1 is between 0.8 and 0.9, then as the temperature is raised (vertical line), the Fe$_3$O complex experiences a first-order phase transition at $\sim$112 K from phase I to phase II. Further increase in the temperature of the Fe$_3$O complex leads to a higher order phase transition from phase II to III starting at $\sim$113 K and culminating at $\sim$190 K. On the other hand, the Mn$_3$O complex has a different magnitude of the J_2/J_1 ratio. If J_2/J_1 is less than $\sim$0.78, then upon an increase in temperature the Mn$_3$O complex will convert directly from phase I to phase III via a first-order phase transition.

In summary, it is amazing how cooperatively the valence detrapping occurs in [Mn$_3$O(O$_2$CCH$_3$)$_6$(py)$_3$]·py. Appreciable intermolecular interactions in the form of both py···py and Mn$_3$O···S

contacts must exist. There is a sudden change in solvate molecules from static to dynamic that occurs at the phase transition. Molecular mechanics calculations should be performed to evaluate with known crystallographic coordinates what potential fields the solvate molecules experiences in these M_3O complexes. There is a possibility that small van der Waals interactions ($\sim$50–100

cm^{-1}) between the M_3O and S molecules valence-trap the M_3O complexes.[6k]

Synthesis and Structure of Dirhodium Compounds Featuring an End-On-Bridging Ditellurium

Massimo Di Vaira,*,[†] Maurizio Peruzzini,[‡] and Piero Stoppioni*,[†]

The reaction of a polytellurides solution with (np₃)Rh and (pp₃)Rh cationic species [np₃ = tris(2-(diphenylphosphino)ethyl)amine, $N(CH_2CH_2PPh_2)_3$; pp₃ = tris(2-(diphenylphosphino)ethyl)phosphine, $P(CH_2CH_2PPh_2)_3$] yields the compounds [LRh]₂Te₂·THF [L = np₃ (**1**), pp₃ (**2**); THF = tetrahydrofuran]; the pp₃ derivative crystallizes also without solvent: [(pp₃)Rh]₂Te₂ (**3**). The polytellurides solution is easily prepared by reducing tellurium in aprotic solvents. The crystal structures of **1**–**3** were elucidated through complete X-ray analyses. The isomorphous compounds **1** and **2** crystallize in the monoclinic space group $P2_1/n$ with Z = 2 and the following lattice constants: (**1**) a = 13.532 (4) Å, b = 19.669 (6) Å, c = 14.492 (9) Å, β = 91.89 (7)°; (**2**) a = 13.598 (9) Å, b = 20.243 (6) Å, c = 14.492 (5) Å, β = 92.55 (4)°. Compound **3** is triclinic $P\bar{1}$, with a = 13.543 (2) Å, b = 13.716 (3) Å, c = 13.370 (4) Å, α = 111.65 (2)°, β = 95.62 (2)°, γ = 119.05 (2)°, and Z = 1. All complexes contain a Te₂ unit end-on bound to two rhodium–ligand fragments forming a zigzag Rh–Te–Te–Rh chain. The isomorphous compounds **1** and **2** exhibit essentially identical [2.691 (2) Å] Te–Te distances. Changes in packing between the former compounds and **3** result in an appreciable change in that distance, which lengthens to 2.760 (1) Å.

Introduction

The chemistry of transition-metal compounds containing unsubstituted chalcogen atoms is currently opening new prospects in various fields. A rapidly growing class of chalcogen-rich metal compounds that exhibit unusual structural and reactivity patterns has been obtained by allowing appropriate metal fragments to react with elemental chalcogens or their derivatives. An important role is played by such compounds in the metal assisted synthesis of "chalcogenospecific" sulfur and selenium heterocycles[1] and Me₂C-substituted polysulfanes.[2] Moreover, they are of interest for applications ranging from the field of catalysis[3] to that of dry lubricants.[4] Also, it has recently been shown that organometallic chalcogenides may provide parent compounds for inorganic solid-state products under mild conditions.[5]

The chemistry of polysulfides[6–8] is reasonably well developed; several polyselenides[9–11] have also been reported. However, up to now the chemistry of tellurium in transition-metal compounds has received less attention. Some compounds containing a tellurium atom either at a vertex of a tetrahedral[12] or octahedral[13] frame or in a bridging position between two or three metal fragments have been described.[14] In the latter compounds, single or double tellurium to metal bonds are considered to exist according to the electronic requirements of the metal atoms. Only two examples of metal complexes containing tri-[15] or tetra-tellurium[16] moieties have been characterized, whereas a few transition-metal compounds containing the ditellurium unit have been described.[17–20] The Te₂ unit is generally linked to two or three metal fragments, one of which is always side-on bonded; the other fragments, when present, are either side-on[18] (I) or terminally[17,19] (II) bound. The geometric arrangements arising about Te₂ are as those illustrated in Chart I. Such arrangements point to a preference for side-on coordination and high connectivity by ditellurium in transition-metal compounds; the same propensity is exhibited by ditellurium in transition-metal carbonyl clusters.[21] The existence of stable monomeral LNiTe₂ (III) compounds [L = 1,1,1-tris((diphenylphosphino)methyl)ethane (triphos), bis-

Chart I

I M = (triphos)Ni[18a]
(PMe₃)₃Co[18b]

II M = Cp*Re(CO)₂[19]   M = W(CO)₅[17]

III M = (triphos)Ni, (ppp)Ni[20]

ppp = PhP(CH₂-PPh₂)₂

triphos = CH₃-C(CH₂-PPh₂)₃
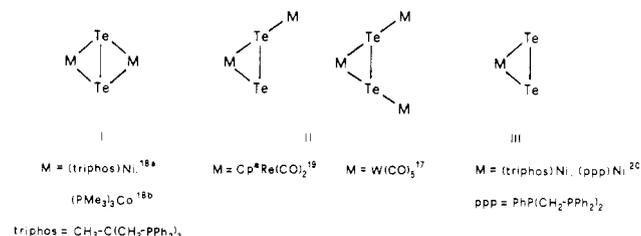
(2-(diphenylphosphino)ethyl)phenylphosphane (p₃)],[20] which easily add $(ML)^{2+}$ to form type I compounds, confirms, on the one hand,

(1) Giolando, D. M.; Papavassiliou, M.; Pickardt, J.; Rauchfuss, T. B.; Steudel, R. *Inorg. Chem.* **1988**, *27*, 2596.
(2) Steudel, R.; Strauss, R.; Jensen, D. *Chem.-Ztg.* **1985**, *109*, 349.
(3) Pohl, F. A.; Bohm, H. U.S. Patent 3 907 600, 1975.
(4) Rouxel, J.; Brec, R. *Annu. Rev. Mater. Sci.* **1986**, *16*, 137.
(5) Steigerwald, M. L.; Rice, C. E. *J. Am. Chem. Soc.* **1988**, *110*, 4228.
(6) Draganjac, M.; Rauchfuss, T. B. *Angew. Chem., Int. Ed. Engl.* **1985**, *24*, 742.
(7) Vahrenkamp, H. In *Sulfur*; Müller, A., Krebs, B., Eds.; Elsevier: Amsterdam, 1984; p 121.
(8) Diemann, E.; Müller, A. *Coord. Chem. Rev.* **1976**, *10*, 79.
(9) Gysling, H. J. In *The Chemistry of Organic Selenium and Tellurium Compounds*; Patai, S., Rappaport, Z., Eds.; Wiley: New York, 1986; p 680.
(10) Shaver, A.; McCall, J. M. *Organometallics* **1984**, *3*, 1823.
(11) Wardle, R. W. M.; Chau, C. N.; Ibers, J. A. *J. Am. Chem. Soc.* **1987**, *109*, 1859.
(12) Strause, C. E.; Dahl, L. F. *J. Am. Chem. Soc.* **1971**, *93*, 6032.
(13) (a) Bogan, L. E.; Lesch, D. A.; Rauchfuss, T. B. *J. Organomet. Chem.* **1983**, *250*, 429. (b) Ryan, C. R.; Dahl, L. F. *J. Am. Chem. Soc.* **1975**, *97*, 6905.
(14) Herrmann, W. A. *Angew. Chem., Int. Ed. Engl.* **1986**, *25*, 56.
(15) (a) Faggiani, R.; Gillespie, R. J.; Campana, C.; Kolis, J. W. *J. Chem. Soc., Chem. Commun.* **1987**, 485. (b) Seigneurin, A.; Makani, T.; Jones, D. J.; Roziere, J. *J. Chem. Soc., Dalton Trans.* **1987**, 2111.
(16) Flower, W. A.; O'Neal, S. C.; Kolis, J. W.; Jeter, D.; Cordes, A. W. *Inorg. Chem.* **1988**, *27*, 971.
(17) Scheidsteger, O.; Huttner, G.; Dehnicke, K.; Pebler, J. *Angew. Chem., Int. Ed. Engl.* **1985**, *24*, 428.
(18) (a) Di Vaira, M.; Peruzzini, M.; Stoppioni, P. *J. Chem. Soc., Chem. Commun.* **1986**, 384. (b) Klein, H. F.; Gass, M.; Koch, V.; Eisenmann, B.; Schäfer, H. *Z. Naturforsch.* **1988**, *43B*, 830.

†Università di Firenze.
‡Istituto ISSECC, CNR.